Journal of Integrative Neuroscience

J. Integr. Neurosci. **2026**; 25(9): 52398
https://doi.org/10.31083/JIN52398

Original Research

Paraventricular Hypothalamic GLP-1R Neurons Mediate Propofol-Induced Suppression of Food Intake

Jun Liang[1,2,†], Mingzhan Yin[1,2,†], Yang Su[1,2], Libo Zhang[1,2], Yong Han[1,2,*]

[1]Department of Endocrinology, Songjiang Research Institute, Songjiang Hospital Affiliated to Shanghai Jiao Tong University School of Medicine, 201699 Shanghai, China
[2]Shanghai Key Laboratory of Emotions and Affective Disorders (LEAD), Shanghai Jiao Tong University School of Medicine, 201699 Shanghai, China
*Correspondence: hanyong@shsmu.edu.cn (Yong Han)
[†]These authors contributed equally.

Academic Editor: Jose Donato Junior
Submitted: 30 March 2026 Revised: 3 May 2026 Accepted: 12 May 2026 Published: 15 September 2026

Abstract

Background: Propofol is a widely used intravenous anesthetic, yet its impact on post-anesthetic feeding remains poorly characterized. The paraventricular nucleus of the hypothalamus (PVN) plays a key role in satiety regulation via glucagon-like peptide-1 receptor (GLP-1R) signaling. This study investigated whether $PVN^{GLP\text{-}1R}$ neurons mediate propofol-induced suppression in food intake. **Methods:** Food intake was measured in wild-type mice following different doses of propofol (25, 50, 100 mg/kg, i.p.) under different conditions (hunger, day and night). The neuronal activation during the period of feeding suppression by anesthesia was assessed via c-Fos immunohistochemistry. In *Glp1r-Cre* mice, $PVN^{GLP\text{-}1R}$ neurons were selectively activated or inhibited using optogenetics to determine their role in post-anesthetic feeding behavior. Fiber photometry with the calcium indicator GCaMP8m was used to record their activity in response to feeding onset during the recovery. Neural circuits were mapped using rabies virus (retrograde tracing) and synaptophysin-based virus (anterograde tracing). **Results:** An anesthetic dose of propofol (100 mg/kg, i.p.) suppressed food intake, regardless of circadian phase or metabolic state, whereas subanesthetic doses of propofol yielded inconsistent results depending on different scenarios. Propofol anesthesia increased c-Fos expression in $PVN^{GLP\text{-}1R}$ neurons. Fiber photometry revealed that propofol abolished the physiological decrease in $PVN^{GLP\text{-}1R}$ neuronal activity during food intake. The optogenetic activation of these neurons suppressed food intake, whereas inhibition promoted food intake in the post-anesthetic recovery period. Viral tracing revealed the upstream and downstream targets of $PVN^{GLP\text{-}1R}$ neurons and confirmed bidirectional connections between $PVN^{GLP\text{-}1R}$ neurons and the key appetite-related nuclei, including the lateral septum (LS), paraventricular thalamus (PVT), arcuate nucleus (ARC) and nucleus tractus solitarius (NTS). **Conclusions:** $PVN^{GLP\text{-}1R}$ neurons are essential mediators of the propofol-induced suppression of food intake.

Keywords: glucagon-like peptide-1 receptor; feeding behavior; paraventricular hypothalamic nucleus; propofol

1. Introduction

Propofol is a commonly used intravenous anesthetic in clinical practice, characterized by a rapid onset, a short duration of action, and minimal side effects. The existing research on this formulation primarily focuses on areas such as anesthesia and inflammation [1,2]. In contrast, its impact on post-anesthetic food intake remains underinvestigated. The sedative and anesthetic effects of propofol are mainly mediated by potentiating the γ-aminobutyric acid (GABA)-A receptor's function [3,4]. Furthermore, propofol exhibits non-hypnotic effects, including anxiolytic [5], antidepressant [6], and antiemetic [7]. Regarding its effect on food consumption, the existing evidence remains contradictory. Some studies support its appetite-stimulating properties [8,9,10] while others report no significant effect beyond sedation [11]. Given the increasing importance of postoperative nutritional recovery [12], clarifying the effects of propofol on feeding behavior has important clinical relevance.

The hypothalamus integrates food-related signals for metabolic control [13,14,15], primarily through key nuclei—such as the arcuate nucleus (ARC) [16,17], the dorsomedial hypothalamus (DMH) [18,19], and paraventricular nucleus of the hypothalamus (PVN) [20]—critical for processing these signals. These nuclei express receptors for crucial metabolic hormones, including leptin, ghrelin, insulin, and glucagon-like peptide-1 (GLP-1), all of which are central in regulating food intake [21,22,23,24,25]. GLP-1 acts via the GLP-1 receptor (GLP-1R), an important member of G protein-coupled receptor (GPCR) family [26,27]. GLP-1 is an incretin hormone secreted mainly by intestinal L-cells [28,29,30]; however, it is also synthesized in discrete brainstem nuclei and acts to suppress feeding [31]. GLP-1R is expressed in the PVN [22]. The activation of the nucleus tractus solitarius (NTS)-to-PVN GLP-1 pathway is sufficient to suppress food intake. Likewise, GLP-1R signaling impairment in the PVN promotes obesity [32]. Conversely, selective pharmacological blockade of GLP-1R in the PVN increases food consumption and promotes weight

gain [33]. However, the functional relationship between propofol anesthesia and GLP-1R signaling in the PVN remains unexplored.

This study investigates whether and through what mechanisms $PVN^{GLP\text{-}1R}$ neurons mediate the effects of propofol anesthesia in relation to feeding behavior. To address this, we use *Glp1r-Cre* mice to monitor real-time activity dynamics of these neurons via *in vivo* fiber photometry and functionally interrogate their role through optogenetic stimulation and inhibition during and after propofol exposure. Collectively, these studies reveal a previously unrecognized neural pathway by which propofol engages satiety circuitry, and may have implications for perioperative nutritional management.

2. Materials and Methods

2.1 Chemicals and Reagents

For immunohistochemistry, the following primary antibodies were used: rabbit anti-GLP-1R antibody (1:800, Abcam, #ab218532, Cambridge, MA, USA) and rat monoclonal antibody against c-Fos (1:1000, Synaptic Systems, #226 017, Göttingen, Germany). The corresponding secondary antibodies were goat anti-rabbit IgG conjugated to Alexa Fluor 488 (1:500, Abcam, #ab150077) and donkey anti-rat IgG conjugated to Cy3 (1:500, Jackson ImmunoResearch, #712-165-153, West Grove, PA, USA). Tissues were permeabilized and blocked with a solution containing 0.2% Triton X-100 (Sangon Biotech, #A110694-0100, Shanghai, China) and a commercial blocking buffer (Beyotime Institute of Biotechnology, #P0260, Shanghai, China).

Propofol (MedChemExpress, Monmouth Junction, NJ, USA; catalog no. HY-B0649; purity 99.52%) was initially dissolved in dimethyl sulfoxide (DMSO) (D8418, Sigma-Aldrich, St. Louis, MO, USA) to prepare a stock solution, which was subsequently diluted in 20% (*w/v*) sulfobutylether-β-cyclodextrin (SBE-β-CD; MedChemExpress, HY-17031) immediately prior to the intraperitoneal injection.

For the RNAscope *in situ* hybridization, target-specific probe sets targeting *Glp1r* (Mm-Glp1r-C1, #418851), *Vgat* (Mm-Vgat-C3, #319191), and *Vglut2* (Mm-Vglut2-C2, #319171) were purchased from Advanced Cell Diagnostics (ACD, a Bio-Techne brand, Newark, CA, USA).

2.2 Animals

Adult (8–12-week-old) male C57BL/6 mice and Glp1r-Cre mice were used. For food intake measurements, mice were singly housed under a 12 h light/dark cycle (lights on at 07:00) at a constant temperature of 24 ± 2 °C with ad libitum access to food and water, except where food restriction was applied. All procedures were approved by the Institutional Animal Care and Use Committee of the Shanghai Jiao Tong University School of Medicine.

2.3 Study Protocol

To evaluate the effects of propofol on food consumption, food intake was assessed in wild-type mice following intraperitoneal injection of propofol (25, 50, or 100 mg/kg) or vehicle (DMSO) administration under three conditions: (1) Daytime feeding (10 a.m. injection); cumulative food intake measured at 1, 2, 4, 6, 8, and 24 h over 24 h (10:00–10:00); (2) Fasted refeeding: 18-h overnight fasting (16:00–10:00), measured the same as in daytime; (3) Nighttime feeding (7 p.m. injection); intake measured at 1, 2, 4, and 12 h during the dark phase (19:00–07:00). The righting reflex was assessed by placing mice in a supine position. The loss of righting reflex (LORR) was defined as the failure to regain upright posture within 30 s after being placed supine and the return of righting reflex (RORR) was recorded when the mice regained a prone posture.

To identify brain regions activated during propofol-induced feeding suppression, wild-type mice received propofol (100 mg/kg, i.p.) and were transcardially perfused 2 h later for c-Fos immunohistochemistry. In *Glp1r*-Cre mice, basal food intake was assessed over two consecutive dark-phase hours (19:00–20:00) with 470-nm light pulses (20 Hz, 1.5 mW, 2-s on/1-s off), followed by a post-stimulation period (20:00–21:00) without light. For inhibition experiments, baseline food intake was measured during the light phase: a stimulation period (10:00–11:00) with 470-nm light pulses (1.5 mW, continuous mode, 1-min on/1-min off), followed by a post-stimulation period (11:00–12:00) without light.

Following propofol administration, neurons were optogenetically activated with 470-nm light (1.5 mW) to assess the latencies to LORR and RORR. Mice failing to achieve LORR within 5 min after propofol injection were excluded. Final group sizes of $n = 5$ (control) and $n = 6$ (activation).

For post-anesthetic feeding experiments, $PVN^{GLP\text{-}1R}$ neurons were inhibited using the closed-loop stimulation protocol (470-nm, 1.5 mW, continuous mode) that the stimulation was triggered only the mice were recognized in initiation of a feeding bout. Total food intake was measured over 8 h following propofol administration.

2.4 Stereotaxic Surgeries

Mice were anesthetized with isoflurane (3–5% induction, 1.5% maintenance; R510-22, RWD Life Science Co., Ltd., Shenzhen, China). After confirming anesthesia by tail pinch, the mice were placed in the stereotactic frame (68055, RWD Life Science Co., Ltd.). During anesthesia, the eyes were protected with ophthalmic ointment (H37022025, Shandong Chenxin Fodu Pharmaceutical Co., Ltd., Jining, Shandong, China). During surgeries, a feedback heater (SA416, SansBio, Nanjing, Jiangsu, China) was used to maintain the core body temperature at 36 ± 1 °C. The scalp was locally sterilized, and the skin was incised to remove excess periosteal tissue. A hole with a diameter

of 2 millimeters was drilled in the target area using a high-speed micro-drill (78001, RWD Life Science Co., Ltd). A glass microinjection pipette (BF150-86-10, Sutter Instrument, Novato, CA, USA) was slowly inserted into the PVN (anteroposterior (AP) –0.82, lateral 0.25 and dorsoventral (DV) –4.85 mm). The viruses were injected at a rate of 60 nL/min using an injection pump (R-480, RWD Life Science Co., Ltd.). After each injection, the micropipette was held in place for 10 min before being gradually retracted. The scalp was closed with surgical sutures or dental cement. For fiber photometry recording, the single fiber implant was located higher above the injection sites (medial–lateral (ML) = 0.25 mm, AP = –0.82 mm, and DV = –4.8 mm), and the implant was secured to the skull with dental cement. For optogenetics manipulation, the single fiber implant was higher above the injection sites (ML = 0.25 mm, AP = –0.82 mm, and DV = –4.65 mm). Before conducting the behavioral experiment, the mice were allowed to recover for at least three weeks.

2.5 Viruses

AAV-EF1α-DIO-eGFP (Cat# H3303) was purchased from OBIO Technology (Shanghai, China). AAV2/9-hSyn-DIO-hChR2 (H134R)-P2A-EGFP (BC-0627/9), AAV/9-hSyn-DIO-stGtACR2-EGFP (BC-1228), AAV/9-EF1α-DIO-mRuby-T2A-Synaptophysin-EGFP (BC-1025), AAV/9-EF1α-DIO-N2cG (BC-0442), AAV/9-EF1α-DIO-EGFP-T2A-TVA (BC-0041), and EnvA G-Deleted Rabies-mCherry (BC-RV-CVS-EnvA471) were purchased from Wuhan Brain Case Technology Co., Ltd (Wuhan, Hubei, China). AAV2/5-EF1a-DIO-JGcamp8m-WPRE (PT-9054) was purchased from BrainVTA (Wuhan, Hubei, China). All viral vectors were aliquoted and stored at –80 °C until use.

2.6 In Vivo Fiber Photometry

Fiber photometry recordings were performed three weeks after intracranial viral delivery of GCaMP to allow for surgical recovery and viral expression. Mice were habituated to handling for one week before data acquisition. During recordings, freely moving animals were connected via implanted optic fiber coupled through ceramic ferrules to fiber-optic patch cables (2U789, Inper Technology, Hangzhou, Zhejiang, China). Animals were habituated to tethering one day before recordings. In the feeding-related calcium recording experiment, mice were recorded under a well-fed condition. Recordings were performed between 15:00 and 19:00. A chow food pellet was placed in the home cage, and the mouse was allowed to approach and consume the pellet. When the mouse grabbed the pellet and initiated biting, the onset of biting was defined as time zero. Calcium signal changes were analysed during the 5 s before and 5 s after the onset.

For GCaMP recordings, the excitation light from a 470-nm light-emitting diode (LED) was band-pass filtered (470/10 nm), reflected by a dichroic mirror, focused through a 20× objective, and coupled to an optical commutator. The excitation light was delivered to the implanted fiber through a 2-m optical fiber at a tip intensity of 40 μW. The GCaMP fluorescence signals were recorded using a fiber photometry system (Inper Technology, Hangzhou, Zhejiang, China). GCaMP was excited using a 488-nm laser, and the emitted fluorescence was collected through the same optical fiber and detected by a photomultiplier tube (PMT). The calcium signals were acquired with InperSignal software (V2.0.15, Inper Technology, Hangzhou, Zhejiang, China). Raw signals were analyzed and processed with InperPlot (V1.6, Inper Technology). For each trial, fluorescence changes (ΔF/F) were calculated as $[(F - F_0)/F_0] \times 100\%$, where F_0 represented the mean baseline fluorescence during a 2-s interval preceding feeding onset. The z-score was calculated as $(F–F_0)/\sigma F$, where F represents the test signal and F_0 and σF are the mean and standard deviation of the baseline signal.

2.7 Immunofluorescent Histochemistry

The mice were deeply anesthetized with 5% isoflurane for approximately 2–3 min until loss of the pedal withdrawal reflex. While under deep anesthesia, the animals were transcardially perfused with ice-cold phosphate-buffered saline (PBS) (B548117, Sangon Biotech, Shanghai, China) followed by 4% paraformaldehyde (PFA) (P39200, Acmec, Shanghai, China). Death was confirmed by the absence of respiration and heartbeat. The brains were rapidly dissected, post-fixed in 4% PFA for 3 h at 4 °C, cryoprotected in 30% sucrose (Sigma-Aldrich, St. Louis, MO, USA) in PBS until saturated (~48 h), embedded in Tissue-Tek® O.C.T. Compound (Cat# 4583, Sakura Finetek, Torrance, CA, USA), and sectioned coronally at 30 μm on a cryotome (CM1950, Leica, Wetzlar, Germany). Immunofluorescence staining was performed as previously described [34]. The brain sections were incubated with the primary antibody overnight, followed by incubation with a secondary antibody solution for 2 h at room temperature. Images were acquired with a laser confocal microscope (FV3000, Olympus, Tokyo, Japan).

2.8 RNAscope In Situ Hybridization

Coronal brain sections (15 μm) were first prepared. Fluorescence *in situ* hybridization was performed using an RNAscope Multiplex Fluorescent Reagent Kit (323100, ACD Bio, Newark, CA, USA) and appropriately designed probes, according to the manufacturer's standard protocol [35]. Before further processing, the tissue sections were baked for 1 h at 60 °C with a hydrophobic barrier around the perimeter of each section. Then, protease digestion was performed in a HybEZ oven at 40 °C for 30 min pretreatment, with slides then hybridized with a prewarmed probe in the HybEZ oven at 40 °C for 2 h. After hybridization, brain sections underwent four steps of signal amplification

and fluorescence labeling. *Slc17a6*, *Slc32a1*, and *Glp1r* are shown in italics due to the measurement of RNA levels.

2.9 Statistical Analysis

Mice were randomly assigned to control and treatment groups. All behavioral tests were conducted in a blinded fashion. The GraphPad Prism 10 software (GraphPad Dotmatics, Boston, MA, USA) was used for all statistical analyses. Throughout the text, measurements are expressed as mean ± SEM. Comparisons between two groups were analyzed using unpaired two-tailed Student's *t*-tests when data satisfied assumptions of normality. For cumulative food intake experiments involving repeated measurements over time, data were analyzed using two-way repeated-measures ANOVA with treatment and time as factors, followed by Sidak's multiple-comparisons test when appropriate. For the optogenetic stimulation experiment, data were analyzed using two-way ANOVA followed by Sidak's multiple-comparisons test when appropriate. Differences were considered statistically significant at $p < 0.05$. Significant differences are indicated in the figures as follows: * $p < 0.05$, ** $p < 0.01$, *** $p < 0.001$ and **** $p < 0.0001$.

3. Results

3.1 Propofol Anesthesia Inhibits Food Intake in WT Mice

To determine whether propofol modulates feeding behavior, wild-type (WT) mice were intraperitoneally injected with propofol at different doses and tested under three feeding conditions: daytime feeding, nighttime feeding, and refeeding after an 18 h overnight fasting. We found that propofol dose (100 mg/kg i.p.) has an obvious inhibitory effect on food intake of chow diet (Fig. 1). Compared with the control group (the injection of an equal volume of solvent), mice in the propofol group consumed significantly less food. During daytime administration (10:00), the propofol revealed a marked suppression at 8 h post-injection ($p = 0.0046$, Fig. 1A). During nighttime administration (19:00), suppression was evident at all measured time points (1 h: $p = 0.004$; 2 h: $p = 0.0006$; 4 h: $p = 0.0007$; 12 h: $p = 0.006$), indicating potent inhibition of nocturnal feeding behavior (Fig. 1B). In 18-h overnight fasted mice, a significant treatment effect was also observed, with a significant reduction at 8 h ($p = 0.046$, Fig. 1C). These results demonstrate propofol anesthesia exerts anorexigenic effects that are strongest during the active phase and weakest during the inactive phase, indicating a critical modulation by circadian timing.

Additionally, to further examine whether the feeding effect of propofol depends on anesthetic depth, we tested the effect of different subanesthetic doses of propofol at different time points (Fig. 1D–I). We found that subanesthetic propofol (25 mg/kg i.p. and 50 mg/kg i.p.) applied during nighttime or under 18 h overnight fasting did not have significant effects on food intake (Fig. 1D–I and Table 1). Under the daytime well-fed condition, 50 mg/kg propofol induced a significant reduction of food intake at 6 h post-injection ($p = 0.009$, Fig. 1G), whereas no sustained effect was observed at the other time points. These findings indicate that the effect of propofol on feeding is dose dependent and is affected by physiological state and circadian rhythm. Among all the tested doses, 100 mg/kg of propofol had the most significant inhibitory effect on food intake, and therefore this dose was used in all subsequent experiments.

Table 1. Effects of different dosage of propofol on food intake under different state and circadian timing.

Dosage	i.p. time	Food intake	Fasted	Anesthesia
25 mg/kg i.p.	10:00	-	NO	NO
50 mg/kg i.p.	10:00	↓	NO	NO
100 mg/kg i.p.	10:00	↓	NO	YES
25 mg/kg i.p	10:00	-	YES	NO
50 mg/kg i.p.	10:00	-	YES	NO
100 mg/kg i.p.	10:00	↓	YES	YES
25 mg/kg i.p.	19:00	-	NO	NO
50 mg/kg i.p.	19:00	-	NO	NO
100 mg/kg i.p.	19:00	↓	NO	YES

↑ increased; ↓ decreased; - no significant change.

3.2 Propofol Anesthesia Activates PVN$^{GLP\text{-}1R}$ Neurons

To elucidate the neural mechanisms underlying propofol-induced suppression of feeding, whole-brain c-Fos screening was performed. The mice were injected with propofol (100 mg/kg, i.p.) at 10:00 and subsequently perfused for c-Fos immunohistochemistry (Fig. 2A). We then identified several brain regions with increased c-Fos expression, including the supraoptic nucleus (SO) and PVN (Fig. 2B). Given that the GLP-1R neurons are subpopulation in the PVN, we next examined whether propofol activates PVN$^{GLP\text{-}1R}$ neurons. Compared with the control group, the propofol group showed a significant increase in the proportion of activated GLP-1R neurons expressing c-Fos in the PVN (Fig. 2C–E), indicating the recruitment of GLP-1R in the PVN by propofol anesthesia. To further identify the neurotype of PVN$^{GLP\text{-}1R}$ neurons, RNAscope was performed for *Glp1r* together with the *Slc32a1* (marker for GABAergic neuron) or *Slc17a6* (marker for glutamatergic neuron). The results showed that PVN$^{GLP\text{-}1R}$ neurons colocalized with both *Slc32a1* and *Slc17a6* (Fig. 2F,G), but these neurons are mainly glutamatergic, with only a small group being GABAergic. In conclusion, these results indicate that propofol anesthesia activates PVN$^{GLP\text{-}1R}$ neurons, which may contribute to the propofol-induced suppression of food intake.

3.3 Propofol Anesthesia Blunts Food-Related Activity of PVN$^{GLP\text{-}1R}$ Neurons

To characterize how PVN$^{GLP\text{-}1R}$ neurons respond to food and whether the activities of these neurons is altered

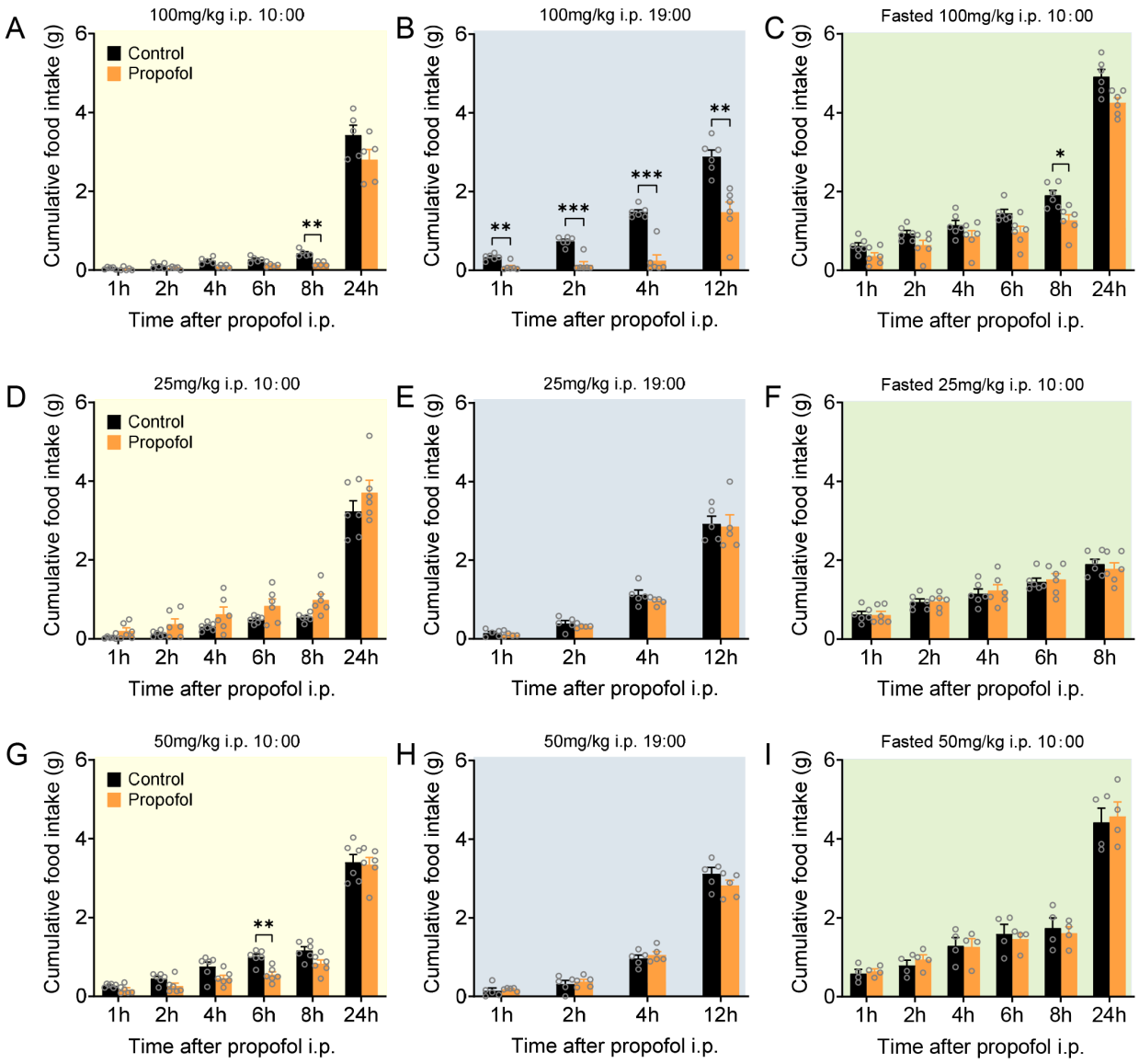

Fig. 1. Propofol regulates food intake in a dose, metabolic state and circadian timing dependent manner. (A,D,G) Daytime food intake following propofol administration at 10:00 under well-fed condition. Mice were received 100 mg/kg (A), 25 mg/kg (D), or 50 mg/kg (G) propofol by i.p. injection, and cumulative food intake was measured at different time points. n = 5–6 per group. (B,E,H) Nighttime food intake following propofol administration at 19:00 under well-fed condition. Mice were received 100 mg/kg (B), 25 mg/kg (E), or 50 mg/kg (H) propofol by i.p. injection, and cumulative food intake was measured at different time points. n = 5–6 per group. (C,F,I) Daytime food intake following propofol administration at 10:00 under fasted condition. Mice were received 100 mg/kg (C), 25 mg/kg (F), or 50 mg/kg (I) propofol by i.p. injection, and cumulative food intake was measured at different time points. n = 4–6 per group. Data are presented as the mean ± standard error of the mean (SEM); two-way repeated-measures analysis of variance (ANOVA) with treatment and time as factors, followed by Sidak's multiple-comparisons test; * $p < 0.05$, ** $p < 0.01$, and *** $p < 0.001$.

by propofol anesthesia, we performed calcium imaging of $PVN^{GLP\text{-}1R}$ neurons in freely moving *Glp1r*-Cre mice injected the AAV-DIO-GCaMP8m into the PVN (Fig. 3A). The viral expression of GCaMP8m in the PVN was confirmed at the end of experiment (Fig. 3B).

First, we examined the neural activities of $PVN^{GLP\text{-}1R}$ neurons in the entire period of propofol anesthesia. As shown in Fig. 3C, intraperitoneal propofol administration induced rapid and sustained suppression of calcium signals in $PVN^{GLP\text{-}1R}$ neurons. Compared with the control, in which neural activities remained relatively high after i.p. injection, propofol induced an obvious reduction of neural activities following injection and attenuated the amplitude of calcium transients. This inhibition persisted throughout

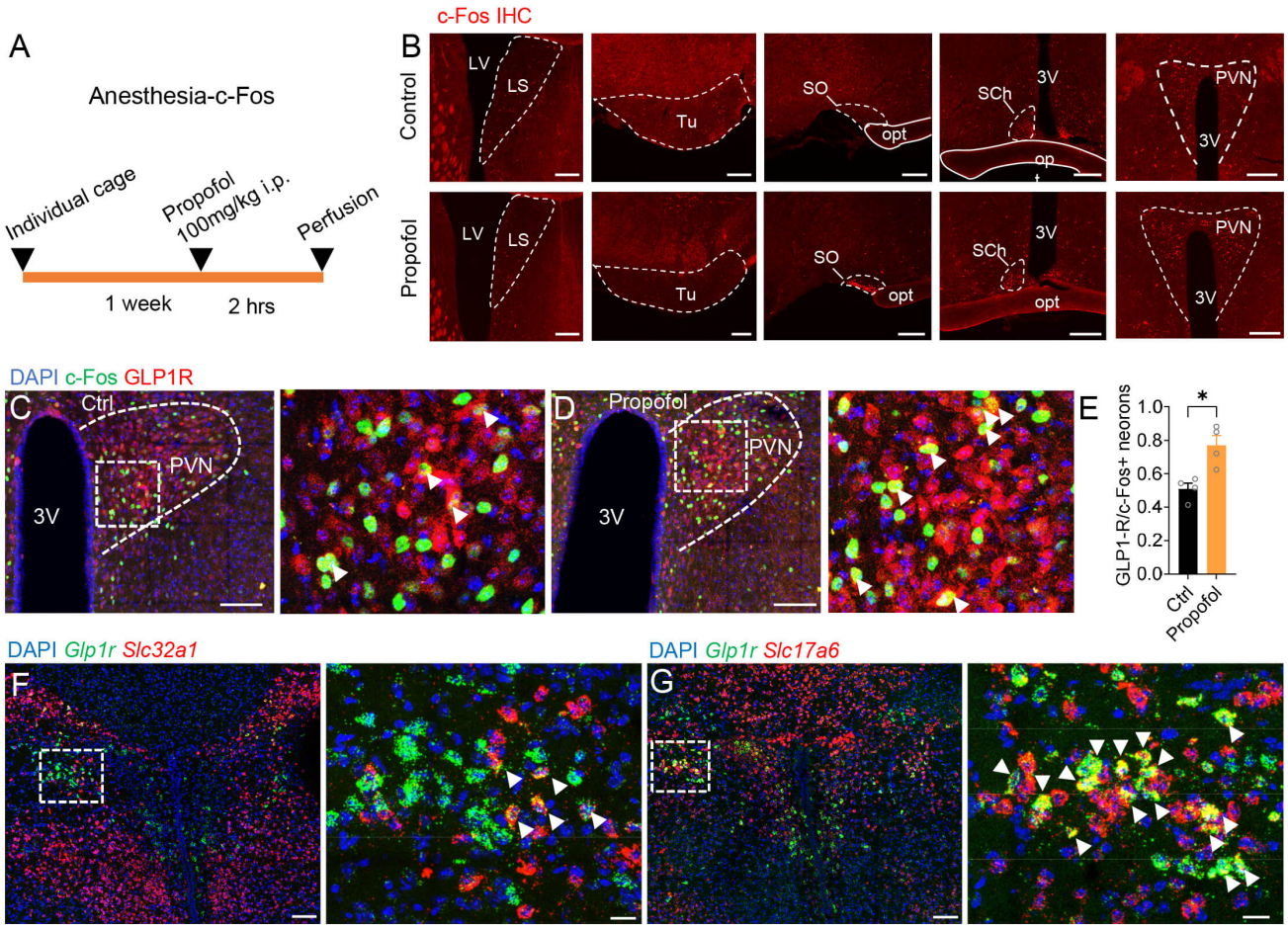

Fig. 2. Propofol anesthesia activates GLP-1R neurons in the PVN. (A) Experimental design of the c-Fos mapping after propofol anesthesia. (B) Representative images showing c-Fos immunostaining from the lateral septum (LS), tuberal area (Tu), supraoptic nucleus (SO), suprachiasmatic nucleus (SCh), and PVN in control and propofol-treated mice. Scale bar, 200 μm. (C,D) Representative images showing the colocalization of $PVN^{GLP\text{-}1R}$ neurons (red) and c-Fos (green) in control (C) and propofol-treated (D) mice. (E) Quantification of the proportion of GLP-1R neurons expressing c-Fos in the PVN. n = 4 per group. Scale bar, 100 μm. (F,G) Representative multiplex RNAscope images showing co-localization of *Glp1r* (green) with *Slc32a1* (red, F) or *Slc17a6* (red, G) in the PVN. Boxed regions are shown at higher magnification on the right panel. Arrowheads indicate co-localized $PVN^{GLP\text{-}1R}$ neurons. Scale bar in (F) and (G), 100 μm. Scale bar in enlarged view, 20 μm. Data are presented as the mean ± SEM; the unpaired *t*-test was used for (E); * $p < 0.05$. GLP-1R, Glucagon-like Peptide-1 Receptor; PVN, Paraventricular Nucleus of the Hypothalamus; LV, lateral ventricle; opt, optic tract; 3V, third ventricle.

the anesthetic period, including the LORR stage and RORR stage. In addition, the sharp increase in signal at the time of injection was attributable to non-specific artifacts introduced by mouse handling and the i.p. injection manipulation, which was observed in the control and propofol group. These results indicate that propofol anesthesia induced a sustained inhibitory effect on $PVN^{GLP\text{-}1R}$ neurons.

Next, we measured the $PVN^{GLP\text{-}1R}$ neuronal activity in response to food during the post-anesthetic recovery period. In the control group, the $PVN^{GLP\text{-}1R}$ neurons showed a change in activity around feeding initiation: calcium signals gradually increased during the pre-feeding period and then sharply decreased at the onset of eating (Fig. 3D). After propofol administration, the dynamic activities of $PVN^{GLP\text{-}1R}$ neurons in the feeding initiation were markedly blunted. In propofol-treated mice, $PVN^{GLP\text{-}1R}$ neurons no longer showed the pre-feeding rise and decrease at eating onset as showed in the control. Instead, calcium activity remained relatively unchanged during the feeding period (Fig. 3E,F), indicating that propofol anesthesia disrupts the normal food-related activity dynamics of $PVN^{GLP\text{-}1R}$ neurons. Given food consumption is associated with a decrease of $PVN^{GLP\text{-}1R}$ neuronal activity, the absence of this inhibition after propofol anesthesia may contribute to propofol-induced suppression of food intake.

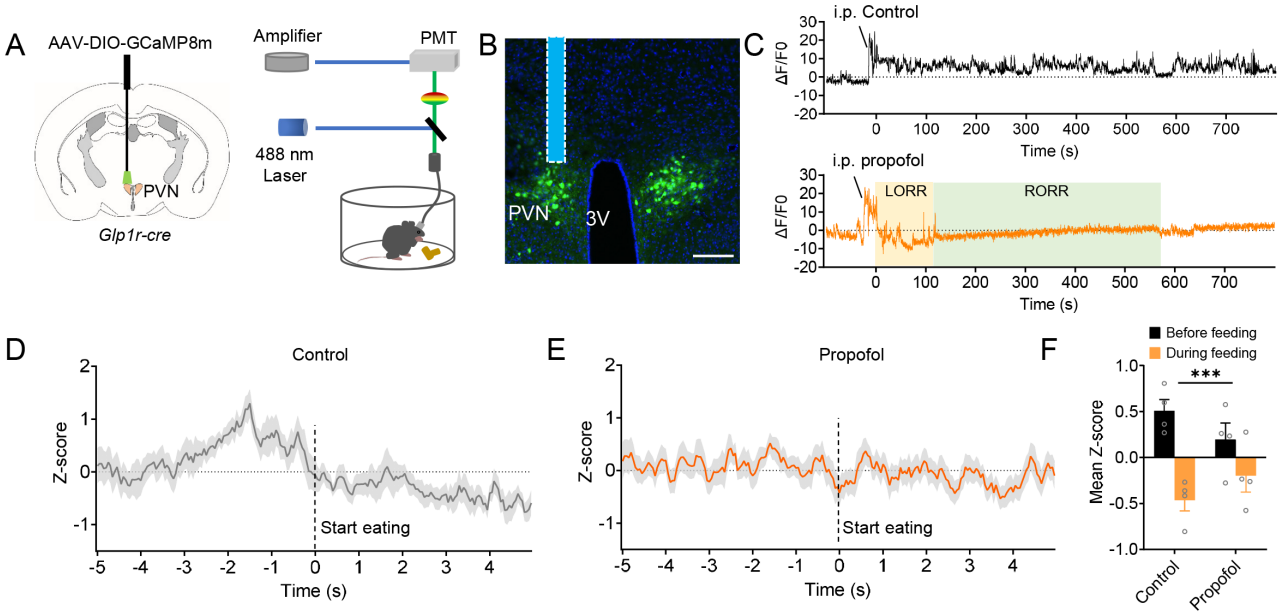

Fig. 3. Propofol anesthesia suppresses the activity and feeding-related dynamics of PVN$^{GLP\text{-}1R}$ neurons. (A) Schematic of the fiber photometry recording in free moving mice. AAV-DIO-GCaMP8m was injected into the PVN of *Glp1r-Cre* mice, and calcium signals from PVN$^{GLP\text{-}1R}$ neurons were recorded through an optical fiber. (B) Representative images showing GCaMP8m expression in the PVN. Scale bar, 200 µm. (C) Representative calcium traces of PVN$^{GLP\text{-}1R}$ neurons following i.p. injection of control or propofol (100 mg/kg). (D,E) Averaged Z-scored calcium activity aligned to eating start in control (D) and propofol-treated (E) mice. (F) Quantification of mean Z-score before and during feeding in control and propofol-treated mice. n = 4 per group. Data are presented as the mean ± SEM; two-way ANOVA followed by Sidak's multiple-comparisons test was used; *** $p < 0.001$ between control and propofol-treated mice. PMT, photomultiplier tube; LORR, loss of righting reflex; RORR, return of righting reflex.

3.4 Optogenetic Activation of the PVN$^{GLP\text{-}1R}$ Neurons Suppresses Feeding and Facilitates Recovery From Anesthesia

Consistent with the previous study on the anorexigenic effect of GLP-1 signaling in the hypothalamus [32], we confirmed that activation of PVN$^{GLP\text{-}1R}$ neurons is sufficient to suppress feeding. The *Glp1r-Cre* mice expressing ChR2 in PVN$^{GLP\text{-}1R}$ neurons were tested during the nighttime (Fig. 4A), when mice exhibit robust food intake. Food intake was measured during two consecutive 1-h periods: a photostimulation period (19:00–20:00) and a subsequent post-stimulation period without light (20:00–21:00) (Fig. 4B). Optogenetic activation of PVN$^{GLP\text{-}1R}$ neurons significantly reduced food intake during the stimulation period compared with control ($p = 0.023$, Fig. 4C). Notably, food intake rebounded significantly in the1 h post-stimulation ($p = 0.015$, Fig. 4C), indicating the suppression of feeding by optogenetics was transient and was followed by a compensatory increase in food consumption.

We then asked whether activation of PVN$^{GLP\text{-}1R}$ neurons affects recovery from propofol anesthesia. *Glp1r-Cre* mice were injected with propofol (100 mg/kg, i.p.) at 10:00, and blue light stimulation was delivered immediately after injection followed by LORR and RORR (Fig. 4D). Optogenetic activation of PVN$^{GLP\text{-}1R}$ neurons tended toward shortening RORR duration and promoted recovery of wakefulness ($p = 0.18$, Fig. 4E), suggesting that these neurons may partially contribute to emergence from anesthesia.

3.5 Optogenetic Inhibition of PVN$^{GLP\text{-}1R}$ Promoted Food Intake After Propofol Anesthesia

We further verified that the optogenetic inhibition of the PVN$^{GLP\text{-}1R}$ could promote feeding behaviors in *Glp1r-Cre* mice (Fig. 4F). Food intake was assessed two consecutive phases in daytime: a 1 h photoinhibition period (10:00–11:00) followed by a 1 h post-stimulation period without light (11:00–12:00) (Fig. 4G). The optogenetic inhibition of the PVN$^{GLP\text{-}1R}$ in daytime significantly increased the food intake ($p < 0.0001$, Fig. 4H).

For post-anesthetic feeding experiments, PVN$^{GLP\text{-}1R}$ neurons were optogenetically inhibited using a closed-loop stimulation protocol, in which light delivery was triggered only when mice were detected at the initiation of a feeding bout. Food intake during post-anesthesia stimulation was monitored for up to 8 h after propofol injection (Fig. 4I). The inhibition of PVN$^{GLP\text{-}1R}$ neurons in the post-anesthesia also increased food intake compared with control ($p = 0.048$, Fig. 4J). These findings indicate that optogenetic inhibition of PVN$^{GLP\text{-}1R}$ neurons promotes post-anesthetic feeding.

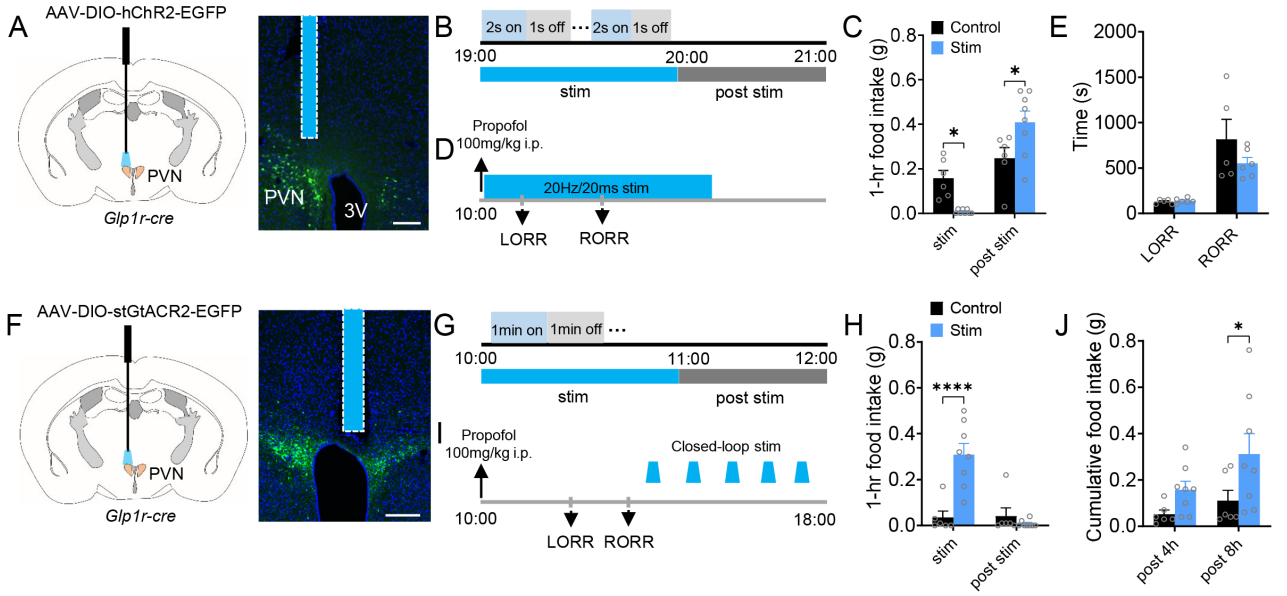

Fig. 4. Bidirectional optogenetic manipulation of PVN$^{GLP\text{-}1R}$ neurons regulates food intake after propofol anesthesia. (A) Schematic of the optogenetic activation of PVN$^{GLP\text{-}1R}$ neurons. AAV-DIO-ChR2-EGFP was injected into the PVN of *Glp1r-Cre* mice, and optical fiber was implanted above the PVN. Representative image showing viral expression in the PVN. Scale bar, 200 μm. (B,D) Experimental design for optogenetic activation in nighttime (B) or daytime after propofol anesthesia (D). (C) Food intake during the 1 h stimulation period and the 1 h post-stimulation period. n = 6–8 per group. (E) Duration of LORR and RORR in control and stimulation groups. n = 5–6 per group. (F) Schematic of the optogenetic inhibition of PVN$^{GLP\text{-}1R}$ neurons. AAV-DIO-stGtACR2-EGFP was injected into the PVN of *Glp1r-Cre* mice, and an optical fiber was implanted above the PVN. Representative image showing viral expression in the PVN. Scale bar, 200 μm. (G,I) Experimental design for optogenetic inactivation in daytime (G) or daytime after propofol anesthesia (I). (H) Food intake during the 1 h stimulation period and the 1 h post-stimulation period. n = 6–8 per group. (J) Cumulative food intake at 4 h and 8 h after propofol injection in control and stimulation groups. n = 6–8 per group. Data are presented as the mean ± SEM; two-way ANOVA followed by Sidak's multiple-comparisons test was used; * $p < 0.05$, **** $p < 0.0001$.

3.6 Afferent and Efferent Projections of the PVN$^{GLP\text{-}1R}$ Neurons

To define the neural connection of PVN$^{GLP\text{-}1R}$ neurons with downstream and upstream targets, we performed both anterograde projection/terminal mapping and monosynaptic rabies-based retrograde tracing (Fig. 5). For the anterograde mapping, we injected AAV-DIO-mRuby-T2A-synaptophysin-EGFP into the PVN of *Glp1r-Cre* mice (Fig. 5A,B). Notably, the use of synaptophysin-EGFP allowed preferential labeling of presynaptic terminals, thereby providing more accurate postsynaptic target regions of PVN$^{GLP\text{-}1R}$ neurons. This approach revealed widespread downstream targets across multiple forebrain, hypothalamic, midbrain, and hindbrain regions (Fig. 5C,G), indicating that PVN$^{GLP\text{-}1R}$ neurons send broad projections to regions involved in feeding, arousal, and behavioral state.

To identify direct inputs to PVN$^{GLP\text{-}1R}$ neurons, we further performed monosynaptic retrograde tracing using a Cre-dependent rabies system. Helper viruses (AAV-DIO-EGFP-TVA and AAV-DIO-N2cG) were first injected into the PVN of *Glp1r-Cre* mice, followed by injection of CVS-EnvA-ΔG-mCherry rabies virus three weeks later (Fig. 5D,E). The mapping results revealed the inputs across multiple brain regions, particularly in the hypothalamus (Fig. 5F,H). We further identified several reciprocal projections originating from PVN$^{GLP\text{-}1R}$ neurons, including the lateral septum (LS), medial preoptic area (MPO), paraventricular thalamus (PVT), SO, bed nucleus of the stria terminalis (BNST), ARC, periaqueductal gray (PAG), and NTS, suggesting that PVN$^{GLP\text{-}1R}$ neurons are an integrative node linking hypothalamic, limbic, and brainstem circuits.

4. Discussion

Propofol remains one of the most widely used intravenous anesthetics in clinical practice [7,36], yet its effect on the recovery of feeding after anesthesia remains unclear. Here, we identify PVN$^{GLP\text{-}1R}$ neurons as an important neuronal population regulating feeding behaviors during the post-anesthetic recovery period. An anesthetic dose of propofol suppressed food intake under different feeding conditions, recruited more GLP-1R-expressing neurons in the PVN. Moreover, propofol anesthesia disrupted the normal feeding-associated dynamics of PVN$^{GLP\text{-}1R}$ neurons that could be partially reversed by optogenetic inhibi-

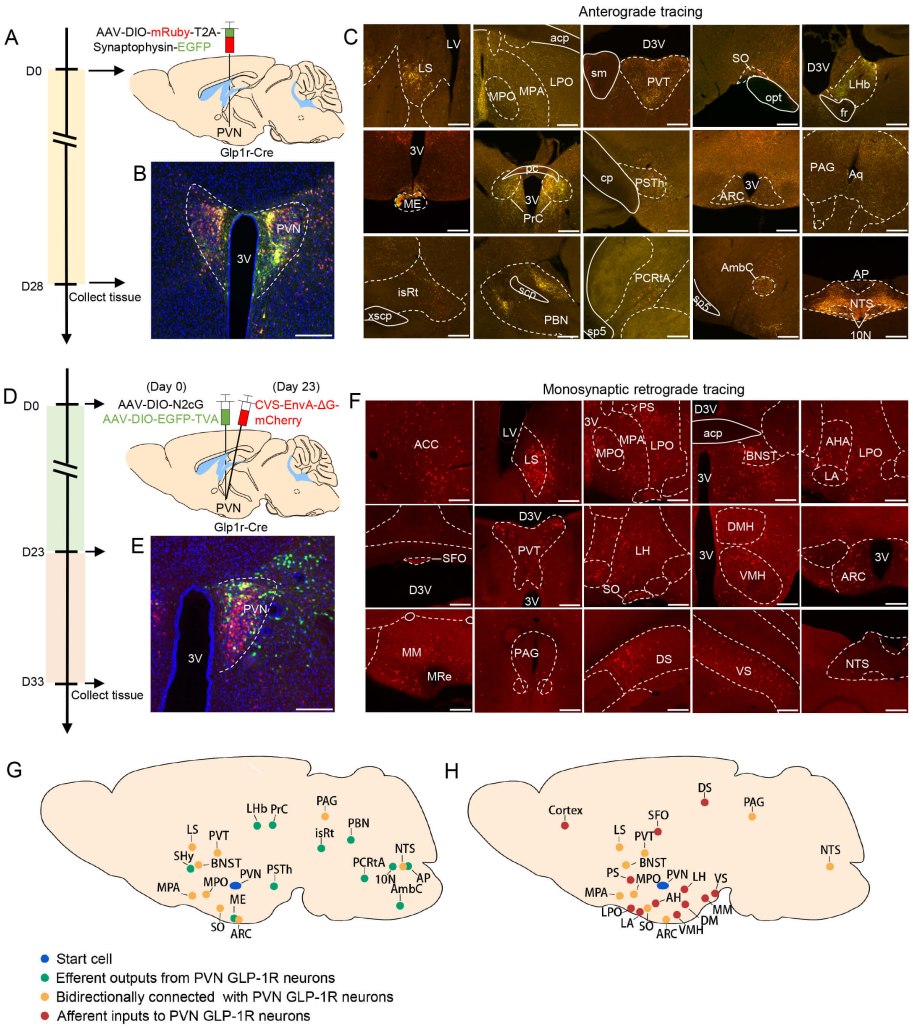

Fig. 5. Afferent and Efferent Projections of the PVN$^{GLP\text{-}1R}$ Neurons. (A) Schematic of anterograde tracing via AAV-DIO-mRuby-T2A-synaptophysin-EGFP injected into the PVN of *Glp1r-Cre* mice. (B) Representative image showing viral expression of mRuby and synaptophysin-EGFP in PVN. Scale bar, 200 μm. (C) Representative coronal sections showing axonal projections of PVN$^{GLP\text{-}1R}$ neurons in multiple brain regions. Scale bar, 200 μm. (D) Schematic of monosynaptic retrograde tracing via AAV-DIO-N2cG and AAV-DIO-EGFP-TVA injected into the PVN of *Glp1r-Cre* mice, followed by injection of CVS-EnvA-ΔG-mCherry rabies virus. (E) Representative image showing the starter cells in the PVN. Scale bar, 200 μm. (F) Representative coronal sections showing monosynaptic inputs to PVN$^{GLP\text{-}1R}$ neurons in multiple brain regions. Scale bar, 200 μm. (G,H) Schematic summary of downstream (G) and upstream (H) projection targets of PVN$^{GLP\text{-}1R}$ neurons. Blue indicates starter cells in the PVN, green indicates efferent projection targets, and orange indicates regions showing bidirectional connectivity with PVN$^{GLP\text{-}1R}$ neurons. acp, anterior commissure, posterior part; MPO, medial preoptic nucleus; LPO, lateral preoptic area; MPA, medial preoptic area; sm, tria medullaris of the thalamus; D3V, dorsal third ventricle; LHb, lateral habenular nucleus; fr, fasciculus retroflexus; ME, median eminence; PrC, precommissural nucleus; cp, cerebral peduncle; PSTh, parasubthalamic nucleus; ARC, arcuate hypothalamic nucleus; PAG, periaqueductal gray; Aq, cerebral aqueduct; isRt, isthmic reticular formation; xscp, decussation of the superior cerebellar peduncle; scp, superior cerebellar peduncle; PBN, parabrachial nucleus; sp5, spinal trigeminal tract; PCRtA, parvicellular reticular nucleus, alpha part; AmbC, ambiguus nucleus, compact part; AP, area postrema; NTS, nucleus tractus solitarius; 10N, dorsal motor nucleus of vagus; ACC, anterior cingulate cortex; BNST, bed nucleus of the stria terminalis; AHA, anterior hypothalamic area; LA, lateroanterior hypothalamic nucleus; SFO, subfornical organ; LH, lateral hypothalamic area; SO, supraoptic nucleus; DMH, dorsomedial hypothalamic nucleus; VMH, ventromedial hypothalamic nucleus; MM, medial mammillary nucleus, medial part; MRe, mammillary recess of the third ventricle; DS, dorsal subiculum; VS, ventral subiculum; ION, inferior olivary nucleus; SHy, septohypothalamic nucleus; AH, anterior hypothalamic area; DM, dorsomedial hypothalamic nucleus; PS, parastrial nucleus.

tion. Together with prior evidence that central GLP-1 signaling and $PVN^{GLP\text{-}1R}$ neurons regulate feeding behavior [31,32,33,37,38], these findings support a model in which $PVN^{GLP\text{-}1R}$ neurons contribute to the delayed recovery of feeding after anesthesia.

The anorexigenic effect of propofol was dose dependent and modulated by metabolic state and circadian timing. Food intake was significantly reduced regardless of propofol (100 mg/kg) administrated during the daytime, nighttime or with fasting. By contrast, subanesthetic doses of propofol (25 or 50 mg/kg) induced weak or inconsistent effects, indicating the anorexigenic effect of propofol is closely associated with the anesthetic state. This dose dependence may help explain the inconsistent literature on propofol and appetite, in which experimental conditions have varied substantially across studies [10]. We also observed that propofol markedly suppressed food intake during the dark period, whereas its effect was much weaker during the light period. This suggests that the feeding effect of propofol may not simply depend on the hunger drive, but may be gated by circadian phase. Circadian rhythms are controlled by the suprachiasmatic nucleus (SCN), which may act through feeding centres including the PVN. Recent studies have shown that SCN neurons can regulate PVN neuronal activity and clock gene rhythms [39,40], and that PVN neurons can show circadian oscillations [41,42]. Therefore, propofol may influence feeding by interfering with SCN→PVN circadian pathway or clock gene expression. This possibility is also supported by previous reports showing that propofol anesthesia can reset circadian timing and downregulate Per1 expression in the SCN [43]. Circadian feeding is increasingly recognized as an important component of energy homeostasis [44], and recent studies suggest pharmacological interventions can modulate feeding behaviors in a circadian phase-dependent manner [45,46].

In control mice, $PVN^{GLP\text{-}1R}$ neurons displayed a consistent transition around feeding onset, with activity increasing before food intake and decreasing at the start of consumption. Anesthetic doses of propofol acutely suppressed calcium activity of $PVN^{GLP\text{-}1R}$ neurons during anesthesia. During the post-anesthetic recovery period, the calcium patterns related to food intake observed in the control group were disrupted, meaning that the normal response to food became blunted. These findings are broadly consistent with the established anorexigenic role of GLP-1 signaling in the PVN [33,37], suggesting that propofol does not merely amplify satiety signal. Instead, it appears to uncouple $PVN^{GLP\text{-}1R}$ neural activity from the temporal dynamics that normally accompanies feeding initiation. The apparent divergence between increased c-Fos expression and blunted calcium activity is not contradictory, given the different temporal resolution of detecting c-Fos and calcium activity [47,48].

GLP-1R related feeding circuits are regulated by multiple feeding-related signals, including ghrelin, leptin, neuropeptide Y (NPY), and neuronal activity in the ARC and parabrachial nucleus (PBN) [49,50,51,52,53]. Therefore, propofol may blunt the normal suppression of $PVN^{GLP\text{-}1R}$ neuronal activity during food intake by regulating these upstream hormonal and neural pathways. First, propofol may alter peripheral feeding-related hormones including neuropeptide Y (NPY), insulin, suggesting that propofol can influence systemic metabolic signals relevant to feeding control. In rats, propofol reduced plasma NPY [54], and in both nonhuman primates and rodents, propofol anesthesia was associated with increased insulin or enhanced GLP-1 production [55,56]. Considering these peripheral hormonal signals can feed back onto hypothalamic and brainstem feeding circuits, this endocrine modulation may represent one mechanism through which propofol influence GLP-1R neuronal activity. Second, propofol may affect hypothalamic and brainstem feeding circuits upstream of PVN neurons, including Agouti-related peptide (AgRP) and proopiomelanocortin (POMC) neurons in the ARC, as well as PBN neurons [57,58]. These circuits provide anorexigenic and orexigenic inputs to PVN neurons and may participate in the rapid neural transition during feeding. Propofol as γ-aminobutyric acid type A ($GABA_A$) receptor agonist, could disrupt the normal neural dynamics of circuit ARC→PVN or PBN→PVN, thereby blocking pre- or postprandial changes in PVN^{GLP1R} neuronal activity.

Activation of $PVN^{GLP\text{-}1R}$ neurons suppressed feeding, whereas inhibition increased food intake under baseline conditions and partly alleviated the post-anesthetic reduction in intake. These bidirectional effects are consistent with prior evidence that GLP-1R signaling in the PVN controls feeding [38,59,60], and further indicate that this genetically defined population contributes directly to the feeding phenotype induced by propofol. Whether this population also contributes to arousal recovery remains less clear. PVN glutamatergic neurons have been implicated in wake regulation [61,62], and our RNAscope data indicate that $PVN^{GLP\text{-}1R}$ neurons are predominantly glutamatergic, with only a small proportion being GABAergic. In the present study, activation of $PVN^{GLP\text{-}1R}$ neurons tended to shorten recovery from propofol, but the effect did not reach significance. We therefore consider $PVN^{GLP\text{-}1R}$ neurons as a subpopulation of governing feeding recovery but not arousal recovery after propofol administration.

Anatomical tracing further defined the circuit framework within which $PVN^{GLP\text{-}1R}$ neurons may regulate postanesthetic feeding. $PVN^{GLP\text{-}1R}$ neurons received monosynaptic inputs from, and projected back to, regions linked to interoceptive and motivational control of feeding, including the LS, PVT, ARC and NTS. The NTS is an important hub in light of prior evidence that brainstem GLP-1 signals engage the PVN to suppress feeding [32,33,63]. Conversely, the broad distribution of GLP-1R expression across brain

regions underscores that $PVN^{GLP\text{-}1R}$ neurons represent one critical node within a GLP-1 signaling network [64]. These anatomical connections provide a neural circuit basis for anesthesia-induced feeding dysregulation, although the validation of individual projections remains pending.

Limitation

This study has several limitations. We examined the role of the overall $PVN^{GLP\text{-}1R}$ neurons in the post-anesthetic feeding. However, this population may contain distinct subtypes, and whether these subpopulations make differential contributions on post-anesthetic feeding will require further investigation. In addition, although anatomical tracing revealed the circuit connectivity of $PVN^{GLP\text{-}1R}$ neurons, the roles of individual inputs and outputs were not tested. Another limitation is that current study does not address potential sex differences. GLP-1 expression differs between sexes [65], and GLP-1-related feeding circuits may be sexually dimorphic [66,67]. And propofol anesthesia may also produce sex-dependent effects on neural activity and metabolism [68,69]. Therefore, whether propofol suppresses feeding through $PVN^{GLP\text{-}1R}$ neurons in female mice remains to be investigated in the future.

Overall, this study establishes $PVN^{GLP\text{-}1R}$ neurons as a key hypothalamic hub that mediates propofol-induced post-anesthetic feeding suppression. These findings not only enhance our understanding of how anesthesia affects feeding, but also may offer a potential basis for improving postoperative nutritional recovery.

5. Conclusions

Propofol suppresses food intake in a dose- and state-dependent manner, and $PVN^{GLP\text{-}1R}$ neurons contribute to this effect. Propofol blunts the normal feeding-related activity dynamics of these neurons, while optogenetic inhibition rescues the post-anesthetic feeding.

Availability of Data and Materials

The datasets used and analyzed during the current study are available from the corresponding author upon reasonable request.

Author Contributions

YH and JL designed the study; JL, MY, YS and LZ conducted the experiments and the data analysis; YH and JL wrote the manuscript; YH supervised all aspects of the project. All authors contributed to editorial changes in the manuscript. All authors read and approved the final manuscript. All authors have participated sufficiently in the work and agreed to be accountable for all aspects of the work.

Ethics Approval and Consent to Participate

All animal experiments were conducted in accordance with the Institutional Animal Care and Use Committee of Shanghai Jiao Tong University School of Medicine and the ARRIVE guidelines 2.0 (see **Supplementary Material**). The research protocol was approved by the Ethics Committee of Shanghai Jiao Tong University School of Medicine (Ethics Approval Number: ACE-003-2023).

Acknowledgment

We gratefully acknowledge the assistance from Songjiang Research Institute Animal Facility and Optical Imaging Core.

Funding

This work was supported by grants from Natural Science Foundation of Shanghai (No. 24ZR1463100 to YH).

Conflicts of Interest

The authors declare no conflicts of interest.

Declaration of AI and AI-Assisted Technologies in the Writing Process

During the preparation of this work, the authors used ChatGPT-5.4 to check spell and grammar. After using this tool, the authors reviewed and edited the content as needed and takes full responsibility for the content of the publication.

Supplementary Material

Supplementary material associated with this article can be found, in the online version, at https://doi.org/10.31083/JIN52398.

References

[1] Gu L, Pan X, Wang C, Wang L. The benefits of propofol on cancer treatment: Decipher its modulation code to immunocytes. Frontiers in Pharmacology. 2022; 13: 919636. https://doi.org/10.3389/fphar.2022.919636

[2] Yi S, Tao X, Wang Y, Cao Q, Zhou Z, Wang S. Effects of propofol on macrophage activation and function in diseases. Frontiers in Pharmacology. 2022; 13: 964771. https://doi.org/10.3389/fphar.2022.964771

[3] Concas A, Santoro G, Serra M, Sanna E, Biggio G. Neurochemical action of the general anaesthetic propofol on the chloride ion channel coupled with GABAA receptors. Brain Research. 1991; 542: 225–232. https://doi.org/10.1016/0006-8993(91)91571-h

[4] Ying SW, Goldstein PA. Propofol suppresses synaptic responsiveness of somatosensory relay neurons to excitatory input by potentiating GABA(A) receptor chloride channels. Molecular Pain. 2005; 1: 2. https://doi.org/10.1186/1744-8069-1-2

[5] Yu L, Zhu X, Peng K, Qin H, Yang K, Cai F, et al. Propofol Alleviates Anxiety-Like Behaviors Associated with Pain by Inhibiting the Hyperactivity of PVN^{CRH} Neurons via $GABA_A$ Receptor β3 Subunits. Advanced Science (Weinheim, Baden-Wurttemberg, Germany). 2024; 11: e2309059. https://doi.org/10.1002/advs.202309059

[6] Zhu XN, Li J, Qiu GL, Wang L, Lu C, Guo YG, et al. Propofol exerts anti-anhedonia effects via inhibiting the dopamine transporter. Neuron. 2023; 111: 1626–1636.e6. https://doi.org/10.1016/j.neuron.2023.02.017
[7] Sahinovic MM, Struys MMRF, Absalom AR. Clinical Pharmacokinetics and Pharmacodynamics of Propofol. Clinical Pharmacokinetics. 2018; 57: 1539–1558. https://doi.org/10.1007/s40262-018-0672-3
[8] Papageorgiou V, Ververidis C, Anagnostou T, Savvas I, Kazakos G. Use of propofol to induce food consumption by anorectic dogs following ovariohysterectomy. Journal of the American Veterinary Medical Association. 2021; 259: 56–61. https://doi.org/10.2460/javma.259.1.56
[9] Fredley V, Kreisler R, Miller K. Subhypnotic dose of intravenous propofol stimulates appetite in cats with stress-induced anorexia. The Veterinary Record. 2020; 187: e58. https://doi.org/10.1136/vr.105740
[10] Besnier E, Clavier T, Tonon MC, Pelletier G, Dureuil B, Castel H, et al. Anesthetic drugs modulate feeding behavior and hypothalamic expression of the POMC polypeptide precursor and the NPY neuropeptide. BMC Anesthesiology. 2018; 18: 96. https://doi.org/10.1186/s12871-018-0557-x
[11] Besnier E, Perdrix A, Gillibert A, Selim J, Froëmer B, Ghemired A, et al. Postoperative hunger after outpatient surgery in patients anesthetized with propofol vs sevoflurane: a randomized-controlled trial. Canadian Journal of Anaesthesia = Journal Canadien D'anesthesie. 2020; 67: 550–559. https://doi.org/10.1007/s12630-020-01584-w
[12] Ljungqvist O, Scott M, Fearon KC. Enhanced Recovery After Surgery: A Review. JAMA Surgery. 2017; 152: 292–298. https://doi.org/10.1001/jamasurg.2016.4952
[13] Schwartz MW, Woods SC, Porte D, Jr, Seeley RJ, Baskin DG. Central nervous system control of food intake. Nature. 2000; 404: 661–671. https://doi.org/10.1038/35007534
[14] Sohn JW, Elmquist JK, Williams KW. Neuronal circuits that regulate feeding behavior and metabolism. Trends in Neurosciences. 2013; 36: 504–512. https://doi.org/10.1016/j.tins.2013.05.003
[15] Saper CB, Chou TC, Elmquist JK. The need to feed: homeostatic and hedonic control of eating. Neuron. 2002; 36: 199–211. https://doi.org/10.1016/s0896-6273(02)00969-8
[16] Aponte Y, Atasoy D, Sternson SM. AGRP neurons are sufficient to orchestrate feeding behavior rapidly and without training. Nature Neuroscience. 2011; 14: 351–355. https://doi.org/10.1038/nn.2739
[17] Jais A, Brüning JC. Arcuate Nucleus-Dependent Regulation of Metabolism-Pathways to Obesity and Diabetes Mellitus. Endocrine Reviews. 2022; 43: 314–328. https://doi.org/10.1210/endrev/bnab025
[18] Imoto D, Yamamoto I, Matsunaga H, Yonekura T, Lee ML, Kato KX, et al. Refeeding activates neurons in the dorsomedial hypothalamus to inhibit food intake and promote positive valence. Molecular Metabolism. 2021; 54: 101366. https://doi.org/10.1016/j.molmet.2021.101366
[19] Yang L, Scott KA, Hyun J, Tamashiro KL, Tray N, Moran TH, et al. Role of dorsomedial hypothalamic neuropeptide Y in modulating food intake and energy balance. The Journal of Neuroscience : the Official Journal of the Society for Neuroscience. 2009; 29: 179–190. https://doi.org/10.1523/JNEUROSCI.4379-08.2009
[20] Li MM, Madara JC, Steger JS, Krashes MJ, Balthasar N, Campbell JN, et al. The Paraventricular Hypothalamus Regulates Satiety and Prevents Obesity via Two Genetically Distinct Circuits. Neuron. 2019; 102: 653–667.e6. https://doi.org/10.1016/j.neuron.2019.02.028
[21] Brüning JC, Fenselau H. Integrative neurocircuits that control metabolism and food intake. Science (New York, N.Y.). 2023; 381: eabl7398. https://doi.org/10.1126/science.abl7398
[22] Shughrue PJ, Lane MV, Merchenthaler I. Glucagon-like peptide-1 receptor (GLP1-R) mRNA in the rat hypothalamus. Endocrinology. 1996; 137: 5159–5162. https://doi.org/10.1210/endo.137.11.8895391
[23] van Dijk G, de Groote C, Chavez M, van der Werf Y, Steffens AB, Strubbe JH. Insulin in the arcuate nucleus of the hypothalamus reduces fat consumption in rats. Brain Research. 1997; 777: 147–152. https://doi.org/10.1016/s0006-8993(97)01103-7
[24] Zigman JM, Jones JE, Lee CE, Saper CB, Elmquist JK. Expression of ghrelin receptor mRNA in the rat and the mouse brain. The Journal of Comparative Neurology. 2006; 494: 528–548. https://doi.org/10.1002/cne.20823
[25] Hâkansson ML, Brown H, Ghilardi N, Skoda RC, Meister B. Leptin receptor immunoreactivity in chemically defined target neurons of the hypothalamus. The Journal of Neuroscience : the Official Journal of the Society for Neuroscience. 1998; 18: 559–572. https://doi.org/10.1523/JNEUROSCI.18-01-00559.1998
[26] Thorens B. Expression cloning of the pancreatic beta cell receptor for the gluco-incretin hormone glucagon-like peptide 1. Proceedings of the National Academy of Sciences of the United States of America. 1992; 89: 8641–8645. https://doi.org/10.1073/pnas.89.18.8641
[27] Graaf CD, Donnelly D, Wootten D, Lau J, Sexton PM, Miller LJ, et al. Glucagon-Like Peptide-1 and Its Class B G Protein-Coupled Receptors: A Long March to Therapeutic Successes. Pharmacological Reviews. 2016; 68: 954–1013. https://doi.org/10.1124/pr.115.011395
[28] Holst JJ. The physiology of glucagon-like peptide 1. Physiological Reviews. 2007; 87: 1409–1439. https://doi.org/10.1152/physrev.00034.2006
[29] Eissele R, Göke R, Willemer S, Harthus HP, Vermeer H, Arnold R, et al. Glucagon-like peptide-1 cells in the gastrointestinal tract and pancreas of rat, pig and man. European Journal of Clinical Investigation. 1992; 22: 283–291. https://doi.org/10.1111/j.1365-2362.1992.tb01464.x
[30] Draghmeh K, Fuehrlein B. Emerging Therapeutics in the Treatment of Substance Use Disorders: A Focus on GLP-1 Receptor Agonists, D3R Antagonists, and CRF Antagonists. Journal of Integrative Neuroscience. 2025; 24: 26361. https://doi.org/10.31083/JIN26361
[31] Holt MK, Richards JE, Cook DR, Brierley DI, Williams DL, Reimann F, et al. Preproglucagon neurons in the nucleus of the solitary tract are the main source of brain GLP-1, mediate stress-induced hypophagia, and limit unusually large intakes of food. Diabetes. 2019; 68: 21–33. https://doi.org/10.2337/db18-0729
[32] Liu J, Conde K, Zhang P, Lilascharoen V, Xu Z, Lim BK, et al. Enhanced AMPA Receptor Trafficking Mediates the Anorexigenic Effect of Endogenous Glucagon-like Peptide-1 in the Paraventricular Hypothalamus. Neuron. 2017; 96: 897–909.e5. https://doi.org/10.1016/j.neuron.2017.09.042
[33] Katsurada K, Maejima Y, Nakata M, Kodaira M, Suyama S, Iwasaki Y, et al. Endogenous GLP-1 acts on paraventricular nucleus to suppress feeding: projection from nucleus tractus solitarius and activation of corticotropin-releasing hormone, nesfatin-1 and oxytocin neurons. Biochemical and Biophysical Research Communications. 2014; 451: 276–281. https://doi.org/10.1016/j.bbrc.2014.07.116
[34] Liu Y, Lin W, Bai Z, Ge Y, Xiao Y, Zhu F, et al. Lcn2 from neutrophil extracellular traps induces astrogliosis and post-stroke emotional disorders. Neuron. 2025; 113: 4199–4216.e8. https://doi.org/10.1016/j.neuron.2025.09.018
[35] Wang H, Wang Q, Cui L, Feng X, Dong P, Tan L, et al. A molecularly defined amygdala-independent tetra-synaptic forebrain-to-hindbrain pathway for odor-driven innate fear and anxiety. Na-

ture Neuroscience. 2024; 27: 514–526. https://doi.org/10.1038/s41593-023-01562-7
[36] Irwin MG, Chung CKE, Ip KY, Wiles MD. Influence of propofol-based total intravenous anaesthesia on peri-operative outcome measures: a narrative review. Anaesthesia. 2020; 75 Suppl 1: e90–e100. https://doi.org/10.1111/anae.14905
[37] Turton MD, O'Shea D, Gunn I, Beak SA, Edwards CM, Meeran K, et al. A role for glucagon-like peptide-1 in the central regulation of feeding. Nature. 1996; 379: 69–72. https://doi.org/10.1038/379069a0
[38] Li C, Navarrete J, Liang-Guallpa J, Lu C, Funderburk SC, Chang RB, et al. Defined Paraventricular Hypothalamic Populations Exhibit Differential Responses to Food Contingent on Caloric State. Cell Metabolism. 2019; 29: 681–694.e5. https://doi.org/10.1016/j.cmet.2018.10.016
[39] Santoso P, Nakata M, Ueta Y, Yada T. Suprachiasmatic vasopressin to paraventricular oxytocin neurocircuit in the hypothalamus relays light reception to inhibit feeding behavior. American Journal of Physiology. Endocrinology and Metabolism. 2018; 315: E478–E488. https://doi.org/10.1152/ajpendo.00338.2016
[40] Jones JR, Chaturvedi S, Granados-Fuentes D, Herzog ED. Circadian neurons in the paraventricular nucleus entrain and sustain daily rhythms in glucocorticoids. Nature Communications. 2021; 12: 5763. https://doi.org/10.1038/s41467-021-25959-9
[41] Van Drunen R, Dai Y, Wei H, Fekry B, Noori S, Shivshankar S, et al. Cell-specific regulation of the circadian clock by BMAL1 in the paraventricular nucleus: Implications for regulation of systemic biological rhythms. Cell Reports. 2024; 43: 114380. https://doi.org/10.1016/j.celrep.2024.114380
[42] Zhao H, Liao M, Huo R, He T, Tian H, Li Z, et al. Restoring circadian rhythms in the hypothalamic paraventricular nucleus reverses aging biomarkers and extends lifespan in male mice. Cell. 2026; 189: 2007–2023.e20. https://doi.org/10.1016/j.cell.2026.01.016
[43] Ben-Hamouda N, Poirel VJ, Dispersyn G, Pévet P, Challet E, Pain L. Short-term propofol anaesthesia down-regulates clock genes expression in the master clock. Chronobiology International. 2018; 35: 1735–1741. https://doi.org/10.1080/07420528.2018.1499107
[44] la Fleur SE, Blancas-Velazquez AS, Stenvers DJ, Kalsbeek A. Circadian influences on feeding behavior. Neuropharmacology. 2024; 256: 110007. https://doi.org/10.1016/j.neuropharm.2024.110007
[45] Wang L, Rakhat Y, Nakata M, Dezaki K, Kuwata H, Zhang B, et al. Circadian feeding promotion by Ninjin'yoeito counteracts frailty in aged mice. The Journal of Physiological Sciences : JPS. 2026; 76: 100062. https://doi.org/10.1016/j.jphyss.2026.100062
[46] Nishimura Y, Mabuchi K, Omura N, Igarashi A, Miura M, Mima N, et al. Fluoxetine Mimics the Anorectic Action of Estrogen and Its Regulation of Circadian Feeding in Ovariectomized Female Rats. Nutrients. 2020; 12: 849. https://doi.org/10.3390/nu12030849
[47] Barros VN, Mundim M, Galindo LT, Bittencourt S, Porcionatto M, Mello LE. The pattern of c-Fos expression and its refractory period in the brain of rats and monkeys. Frontiers in Cellular Neuroscience. 2015; 9: 72. https://doi.org/10.3389/fncel.2015.00072
[48] Zhang Y, Rózsa M, Liang Y, Bushey D, Wei Z, Zheng J, et al. Fast and sensitive GCaMP calcium indicators for imaging neural populations. Nature. 2023; 615: 884–891. https://doi.org/10.1038/s41586-023-05828-9
[49] Zhang W, Waise TMZ, Toshinai K, Tsuchimochi W, Naznin F, Islam MN, et al. Functional interaction between Ghrelin and GLP-1 regulates feeding through the vagal afferent system. Scientific Reports. 2020; 10: 18415. https://doi.org/10.1038/s41598-020-75621-5
[50] Biddinger JE, Lazarenko RM, Scott MM, Simerly R. Leptin suppresses development of GLP-1 inputs to the paraventricular nucleus of the hypothalamus. elife. 2020; 9: e59857. https://doi.org/10.7554/eLife.59857
[51] Secher A, Jelsing J, Baquero AF, Hecksher-Sørensen J, Cowley MA, Dalbøge LS, et al. The arcuate nucleus mediates GLP-1 receptor agonist liraglutide-dependent weight loss. The Journal of Clinical Investigation. 2014; 124: 4473–4488. https://doi.org/10.1172/JCI75276
[52] Alhadeff AL, Baird JP, Swick JC, Hayes MR, Grill HJ. Glucagon-like Peptide-1 receptor signaling in the lateral parabrachial nucleus contributes to the control of food intake and motivation to feed. Neuropsychopharmacology : Official Publication of the American College of Neuropsychopharmacology. 2014; 39: 2233–2243. https://doi.org/10.1038/npp.2014.74
[53] Singh I, Wang L, Xia B, Liu J, Tahiri A, El Ouaamari A, et al. Activation of arcuate nucleus glucagon-like peptide-1 receptor-expressing neurons suppresses food intake. Cell & Bioscience. 2022; 12: 178. https://doi.org/10.1186/s13578-022-00914-3
[54] Chang CL, Tsai YC, Niu CS, Hung SF, Cheng JT. Inhibitory effect of propofol on sympathetic neurotransmission results in changes of plasma neuropeptide Y in rats. Journal of Autonomic Pharmacology. 1996; 16: 29–33. https://doi.org/10.1111/j.1474-8673.1996.tb00353.x
[55] Wu CC, Hung CJ, Wang YY, Lin SY, Chen WY, Kuan YH, et al. Propofol Improved Glucose Tolerance Associated with Increased FGF-21 and GLP-1 Production in Male Sprague-Dawley Rats. Molecules (Basel, Switzerland). 2020; 25: 3229. https://doi.org/10.3390/molecules25143229
[56] Kim JM, Shin JS, Yoon IH, Min BH, Jeong WY, Lee GE, et al. The effect of propofol on intravenous glucose tolerance test in rhesus monkey. Journal of Medical Primatology. 2014; 43: 242–246. https://doi.org/10.1111/jmp.12128
[57] Cabral A, Fernandez G, Tolosa MJ, Rey Moggia Á, Calfa G, De Francesco PN, et al. Fasting induces remodeling of the orexigenic projections from the arcuate nucleus to the hypothalamic paraventricular nucleus, in a growth hormone secretagogue receptor-dependent manner. Molecular Metabolism. 2020; 32: 69–84. https://doi.org/10.1016/j.molmet.2019.11.014
[58] Jhamandas JH, Harris KH, Petrov T, Krukoff TL. Characterization of the parabrachial nucleus input to the hypothalamic paraventricular nucleus in the rat. Journal of Neuroendocrinology. 1992; 4: 461–471. https://doi.org/10.1111/j.1365-2826.1992.tb00194.x
[59] Wang L, Savani RH, Lu Y, Bernabucci M, Luis-Islas J, Park E, et al. State-dependent central synaptic regulation by GLP-1 is essential for energy homeostasis. Nature Metabolism. 2025; 7: 1443–1458. https://doi.org/10.1038/s42255-025-01305-x
[60] Savani RH, Wang L, Lu Y, Le T, Park E, Yang M, et al. Individual paraventricular hypothalamic GLP-1R neurons track ingestion across energy states. iScience. 2025; 28: 114070. https://doi.org/10.1016/j.isci.2025.114070
[61] Chen CR, Zhong YH, Jiang S, Xu W, Xiao L, Wang Z, et al. Dysfunctions of the paraventricular hypothalamic nucleus induce hypersomnia in mice. elife. 2021; 10: e69909. https://doi.org/10.7554/eLife.69909
[62] Liu Y, Li Y, Yang B, Yu M, Zhang X, Bi L, et al. Glutamatergic Neurons of the Paraventricular Nucleus are Critical for the Control of Wakefulness. Neuroscience. 2020; 446: 137–144. https://doi.org/10.1016/j.neuroscience.2020.08.024
[63] Larsen PJ, Tang-Christensen M, Holst JJ, Orskov C. Distribution of glucagon-like peptide-1 and other preproglucagon-derived peptides in the rat hypothalamus and brainstem. Neuroscience. 1997; 77: 257–270. https://doi.org/10.1016/s0306-4522(96)

00434-4
[64] Cork SC, Richards JE, Holt MK, Gribble FM, Reimann F, Trapp S. Distribution and characterisation of Glucagon-like peptide-1 receptor expressing cells in the mouse brain. Molecular Metabolism. 2015; 4: 718–731. https://doi.org/10.1016/j.molmet.2015.07.008
[65] Ryu V, Gumerova A, Pevnev G, Yuen T, Zaidi M. Atlas of GLP-1 expression in the mouse brain: Neuroanatomical basis for metabolic and psychiatric effects. Brain Medicine : from Neurons to Behavior and Better Health. 2026; 2: 21–31. https://doi.org/10.61373/bm026a.0006
[66] López-Ferreras L, Eerola K, Mishra D, Shevchouk OT, Richard JE, Nilsson FH, et al. GLP-1 modulates the supramammillary nucleus-lateral hypothalamic neurocircuit to control ingestive and motivated behavior in a sex divergent manner. Molecular Metabolism. 2019; 20: 178–193. https://doi.org/10.1016/j.molmet.2018.11.005
[67] Bales MB, Centanni SW, Luchsinger JR, Fathi P, Biddinger JE, Le TDV, et al. High fat diet blunts stress-induced hypophagia and activation of Glp1r dorsal lateral septum neurons in male but not in female mice. Molecular Metabolism. 2022; 64: 101571. https://doi.org/10.1016/j.molmet.2022.101571
[68] Choong E, Loryan I, Lindqvist M, Nordling Å, el Bouazzaoui S, van Schaik RH, et al. Sex difference in formation of propofol metabolites: a replication study. Basic & Clinical Pharmacology & Toxicology. 2013; 113: 126–131. https://doi.org/10.1111/bcpt.12070
[69] Gonzales ELT, Yang SM, Choi CS, Mabunga DFN, Kim HJ, Cheong JH, et al. Repeated neonatal propofol administration induces sex-dependent long-term impairments on spatial and recognition memory in rats. Biomolecules & Therapeutics. 2015; 23: 251–260. https://doi.org/10.4062/biomolther.2014.120